4.1 Introduction:

One of the fascinating features of nature's creation is the homochirality of the biological molecules. Most of the biological molecules exist and show their activity in one of the mirror image form, while the other enantiomeric form is incapable of performing. Indeed for many of the biological and pharmaceutical molecules, two enantiomers show markedly different properties. Therefore, synthesis of one of the particular enantiomeric form is of significant importance. Now, this may be achieved either following i) enantioselective synthetic route or ii) separation of a particular enantiomer from racemic mixture. [1,2]

The former method is however more acceptable from a commercial point of view [1,3,4]. A significant number of homogenous catalyst systems are already reported in the literature which allows efficient enantioselective synthesis. In comparison, the heterogeneous catalyst for asymmetric organic transformations has found much less success [5,6]. Studies on fabrication of heterogeneous surfaces capable of asymmetric synthesis have been made through adsorption of optically pure small molecules on various solid material surfaces [7-10]. However these often suffer from the concern of limited stability of the catalyst owing to the possibilities of detachment of chiral molecules leading to a surface of significantly poor chirality. Hence in this purpose, fabrication of chiral catalytic surface by use of strongly bound chiral surface modifier or covalent functionalization of the chiral molecules on the catalyst surface is desirable. In this respect chiral conducting polymers having a specific helicity type should be very much of worth. Moving a few steps further, surfaces made up of chiral conducting polymer may find application in chiral separation, electrochemical detection of chiral molecules and electrochemical asymmetric synthesis. Although the electrochemical asymmetric synthesis has received much less success compared to chemical asymmetric

synthetic methods. Nevertheless, simplicity and cost effective approach of these methods hold huge promise for future applications [11].

Polypyrrole, polythiophene or polyaniline based chiral polymers have received significant attention as chiral conducting polymers. In order to introduce chirality, asymmetric feature needs to be present either in the substrate molecules, reagents, solvents or catalysts. Synthesis of chiral polypyrrole or polythiophene has been carried out by polymerizing corresponding monomers having substituted with asymmetric substituents (enantiopure). The result is formation of polymeric chain with a particular helicity (right or left handed). In an alternative strategy, sense of chirality to the polymeric chains may also be introduced during their doping. Now, it is worth mentioning here that, doping of the conducting polymers is essential for their applications in electrode fabrication, as in the undoped state, conducting polymers behave as semiconductors and only in the doped state they are conducting even upto the metallic regime.

Now, in this respect polyaniline is a very interesting conducting polymer as doping/dedoping of polyaniline is carried out by very much reversible fashion using simple acid base chemistry. In the doped /protonated polycationic state of emaralidine salt, counter anion of acid does the charge balance. Hence, the morphology of the PANI chains in the doped state should significantly depend on the nature of the counter anions. Wallace *et. al.* in 1994 for the first time reported the synthesis of chiral polyaniline where PANI chains of different helicities were produced in presence of (+)HCSA or (-)HCSA as dopants. The helicity of the PANI chains are produced due to supramolecular (H bonding) interactions with the chiral $CSA^{(-)}$ anions. They established the enantioselectivity of the synthetic method by examining the CD spectra of the (+) HCSA or (-) HCSA doped PANI chains, which resulted in mirror image like CD trace

[12]. The chirality of the PANI chains may be induced either by doping of emaraldine base form of PANI by (+) HCSA or (-) HCSA. Similarly, *in situ* doping of PANI chains may also be done by keeping optically pure camphor sulfonic acids present during the chemical oxidative polymerization of aniline. Wallace et al also demonstrated electrochemical oxidation of aniline in presence of enantiopure HCSA to have chiral PANI films on the electrodes.

Apart from providing helicity to the PANI chains, counter anion like $CSA^{(-)}$ also increase processibility of PANI chains in aqueous or various organic solvents. In this respect Wang et al. in 2002 reported water soluble chiral PANI/polyacrylic acid (PAA) nano composites [13]. Choli et. al. reported helicity specific synthesis of chiral nanocomposite with PAA following an enzyme catalytic method [14]. It is however the fact that dopant induced chirality in PANI is a rather secondary method of chirality induction. Therefore, the induced chirality may not be sufficient for various applications as stated above. Thus the chirality of poly pyrrole or polythiophene chains induced by the covalently attached chiral substituents should be superior [15]. However these also suffer from the drawback of relatively poor conductivity of the non conducting chiral substituents present on pyrrole/thiophene nuclei and more difficulties in attaining the mutual coplanarity of the aromatic nuclei owing to the steric hindrance of the substituents. On the other hand the doping by chiral acids and hence inducing chirality in PANI chains is a relatively much easier strategy. Moreover, PANI contains the basic imine nitrogen atoms in the emaralidine base form, which are capable of interacting with acidic functionalities. A major problem in respect of exploiting the reactivity at the said basic 'N' atom centre is the disappearance of chirality after dedoping hence removal of CSA moieties from PANI/CSA composites. However, it was soon realized that dopant induced chirality at the PANI chains could be retained if the dopant removal

is done from the solid films, so that PANI chains do not get the scope for relaxing back to the achiral, randomly coiled conformation. Kaner et. al. used the above as the key principle to get the chiral emaralidine base form and successfully demonstrated the enantiomeric discrimition of D and L–phenylalanine [16]. Sheridan and Breslin carried out the similar amino acid discrimination using electroanalytical technique [17].

Wang and Li in 2004 reported a much improved technique where much higher degree of chirality of the PANI chains observed when the chemical oxidative polymerization of aniline carried out in presence of oligomers of aniline. The oligomers catalyze faster growth of PANI chains by acting as seeds and thus higher degree of chirality of the PANI chains results [18]. The appreciable chirality of PANI nanofibres and their increased surface area promise a significant potential for the fabrication of chiral electrodes. However, relatively poor mechanical stability and moderate conductivity of PANI chains may limit the wide spread application of chiral PANI chains during application as chiral electrodes. In this respect, nanocomposites of chiral PANI chains with carbon based nanomaterials may be promising enough. However, there are only few reports in this field [19,20]. Song and co-workers reported the preparation of noncovalently attached carbon nano tubes (CNT)/PANI chiral composite material [21].

In the present work my objective is to synthesize chiral GO-PANI composites having covalently attached PANI chains. GO nanosheets offer considerable surface area along with significantly high carrier mobility after reduction of GO sheets. Therefore increased conductivity of the composite material coupled with appreciable mechanical properties, both of which are desirable for electrode properties. Chiral PANI chains are grown from the oligoaniline moieties attached covalently with GO sheets in presence of (+) or (-) HCSA as dopants. Thorough analysis of the structure, morphology and impact

of the covalently attached fibriler chiral PANI chains on the energy storage properties has been examined.

4.2. Experimantal Section:

4.2.1. Materials:

Aniline (An), ammonium persulfate (APS), p-phenylenediamine (PPDA), triethylamine (TEA), and dimethylformamide (DMF),Ammonium solution (25%) used in this work are purchased from E-Merck (INDIA) Pvt. Ltd. Camphor sulphonic acid (L-CSA & D-CSA) in this work are purchased from Sigma-Aldrich. Aniline is distilled under reduced pressure and stored at 5^0C in the dark before use. Triethylamine is purified through distillation and. p-phenylenediamine is recrystallised from hot water before use and dialysis is done using a dialysis bag purchased from Sigma-Aldrich with MWCO 12000.

4.2.2. Detailed Method of Preparation:

4.2.2.1. Preparation of GO and GOT:

GO and GOT is prepared similarly as in Chapter 3 [22,23].

4.2.2.2. Synthesis of Covalently attached chiral Polyaniline in presence of Graphene Oxide Surface, GOTPL and GOTPD:

0.2 g (2.1 mmol) of aniline, 5 g of optically active L-CSA (21.4 mmol) and 60 mg of GOT is dispersed in 8 mL of double distilled water, it is stirred over night in inert atmosphere, 0.49 g (2.1 mmol) of ammonium persulfate was dissolved in 2 mL of double distilled water. The solution of APS was added incrementally in ten separate portions to the solution of aniline and LCSA in inert atm. After each addition, the mixed solution was shaken vigorously. The second addition of ammonium persulfate was accomplished after the mixed solution turned from blue to green. The as-synthesized

PANI chiral fibers were characterized by using circular dichroism. D-CSA is used in similar manner, and yield of the product is 230 mg.

4.2.2.3 Synthesis of Non-Covalently Attached Chiral Polyaniline in presence of Graphene Oxide Surface (GOPL):

The above experiment is performed, in presence of 40 mg of GO instead of GOT.

4.2.2.4 Synthesis of Covalently attached Achiral Polyaniline in presence of Graphene Oxide Surface (GOTP):

The same experiment is performed in presences of 60 mg GOT and HCl (equivalent amount of D-CSA).

4.2.3. Characterization:

Analysis of Circular Dichorism spectra is done in JASCO J-815 CD spectrometer. All other characterizations are done like **Chapter 3**.

4.3. Results and Discussion:

The polymerization of aniline in presence of APS as oxidant is carried out at room temperature in aqueous medium. The initiation of the growth of PANI chains induced from the APQD [N,N'-bis(4'-aminophenyl)-1,4-quinonediimine] moieties attached on the GO sheets as in the previous **Chapter 3**. The trimeric aniline moieties present on the GO sheets play dual role here i)These ensure covalent grafting of chiral PANI chains from GO surface, ii) Catalytic effect of trimeric aniline moieties help inducing higher degree of chirality in the PANI chains [18]. Importantly, here about 10 times higher mole ratio of L-HCSA or D-HCSA used for better interaction of the chiral $CSA^{(-)}$ ions with the backbone and simultaneously to suppress the interaction of the PANI chains with achiral SO_4^{2-} ions. In order to have increased rate of aniline polymerization, which has been commented as a very important point for improved

asymmetric induction by Li and Wang, the polymerization reaction is carried out in room temperature with incremental addition of APS as described in experimental section.

4.3.1. Analysis of FTIR Spectra:

The FTIR spectra of GO in **Figure 4.1** shows typically broad absorption for H-bonded hydroxyl groups of carboxylic (OH), phenolic (OH) or alcoholic (OH) group at 3422 cm^{-1}. Expectedly, in GOT the broadness disappears and relatively sharp signal in the similar range is observed which may be attributed to the (N-H) stretching vibration. Interestingly, in case of GOT, the signal at ~1728 cm^{-1} corresponding to the (C=O) stretching for carboxyl group

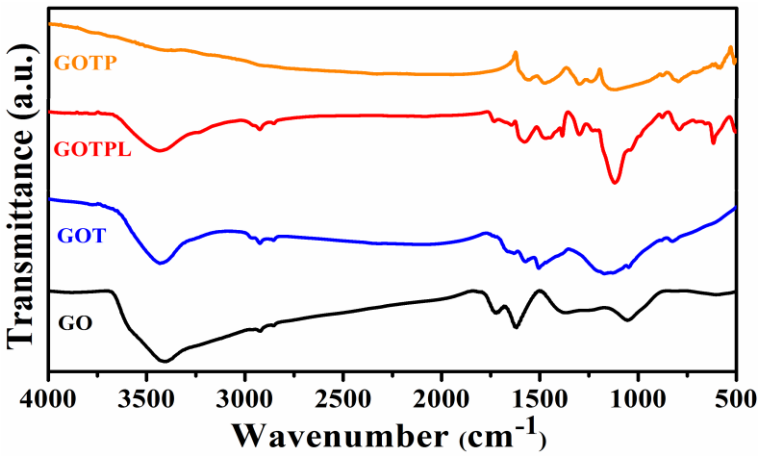

***Figure 4.1**: FTIR spectra for GO, GOT, GOTPL, GOTP samples respectively.*

disappears and a new peak at ~1660 cm^{-1}, signifying the anilide carbonyl group upon attachment of APQD moieties with the (-COOH) groups of GO sheets appear. The broad signal in the range of 1300 cm^{-1} to 1014 cm^{-1} signify all other relatively low energy stretching and bending modes of GO and APQD (as stated in **Chapter 3**). In case of GOTPL, a relatively broad signal at 3422 cm^{-1} which might signify extensively

H-bonded amine groups of PANI chains due to doping with L-HCSA. The relatively less intense signal at 2921 cm^{-1} signify (C-H) stretching of benzenoid or quinonoid rings of PANI chains. The signal at 1736 cm^{-1} probably signify the carbonyl stretching vibration of $CSA^{(-)}$ moieties which is absent in case of GOTP. The (C=C) stretching vibrations for quinonoid and benzenoid rings are observed at 3422 cm^{-1} and 3422 cm^{-1}. The absorptions around 1060 cm^{-1} to 660 cm^{-1} in case of GOTPL confirms the presence of $CSA^{(-)}$ anions produced by doping of PANI chains with HCSA [24]. The bands at 1298 cm^{-1}, 1231 cm^{-1} and 1123 cm^{-1} indicate (C-N) stretching of the secondary aromatic amines and (C-H) bending modes of benzeneoid and quinonoid rings respectively [25-27]. Interestingly, the presence of most intense 'electronic like' bond in the spectrum of GOTPL located at 1123 cm^{-1} indicates higher conductivity expected for this sample compared to GOTP. The higher conductivity might originate due to the extended fiber like morphology in the PANI chains in this sample.

4.3.2. Raman Spectroscopy:

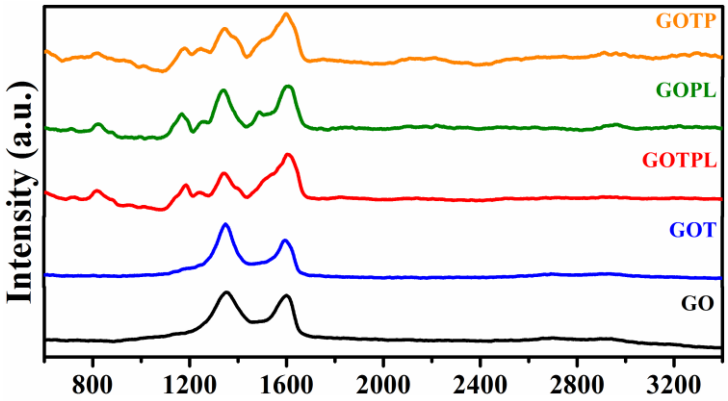

***Figure 4.2**: Raman spectra for GO, GOT, GOTPL, GOTP samples respectively.*

The overlay of Raman spectra in **Figure 4.2** shows appearance of D band corresponding to 1350 cm^{-1} and G band at 1595 cm^{-1} due to doubly degenerate mode of E_{2g} symmetry and originates from the in plane vibration of sp^2 hybridized carbon atoms [28, 29]. The I_D/I_G ratio in case of GOT shows a value of 1.3 increased from 1.06 at a

similar spectra for GO. This obviously indicate increased structural disorder in GOT due to introduction of APQD moieties through the edges of GO sheets and their (π-π) stacking with aromatic rings of GO. In case of GOTPL, the signal at 1595 cm^{-1} for (C=C) stretching vibration and 1345 cm^{-1} for protonated (C-N) stretching vibration overlaps with the D and G bands. The (C=N) stretching vibration~1540 cm^{-1} also comes in overlap with the (C=C) stretching or G band signal. Apart from the other relevant signals of GO and PANI, the above broad signals are very much impressive as those indicate significant interaction of PANI chains with GO surface. It is worth mentioning that the Raman spectrum of GOTP also shows a similar pattern as of GOTPL. However, in case of non covalently attached GO/PANI for GOPL, the broadness are relatively less which possibly indicates lesser interaction between GO sheets and PANI chains.

4.3.3. WAXS Analysis:

The WAXS analysis in **Figure 4.3** shows similar peaks as described in chapter III. In case of GOTPL the signals corresponding to parallel and perpendicular planes of PANI chains are observed at 2θ = 14.79 (011 plane), 19.89 (020 plane) and 25.81 (200 plane) [30]. Apart from these, signals at 2θ = 6.65 and 8.99 probably indicates increased interlayer separation of GO crystallities due to PANI chain formation and interactions. On the other hand, in case of GOPL similar signals for PANI chains are observed at 2θ = 15.55, 21.33 and 25.33 for the above mentioned planes due to parallel and perpendicular planes of PANI. However, apart from these, more sharp signals at 2θ = 16.78, 18.34, 19.23 and 23.34 are observed. The reason behind appearance of these signals is however not clear but formation of $CSA^{(-)}$ induced similar PANI crystanillities due to poor interaction of PANI chains with GO surface may be a potential reason. The poor interaction compared to GOTPL is however expected here due to non covalent attachment of PANI chains and GO surface.

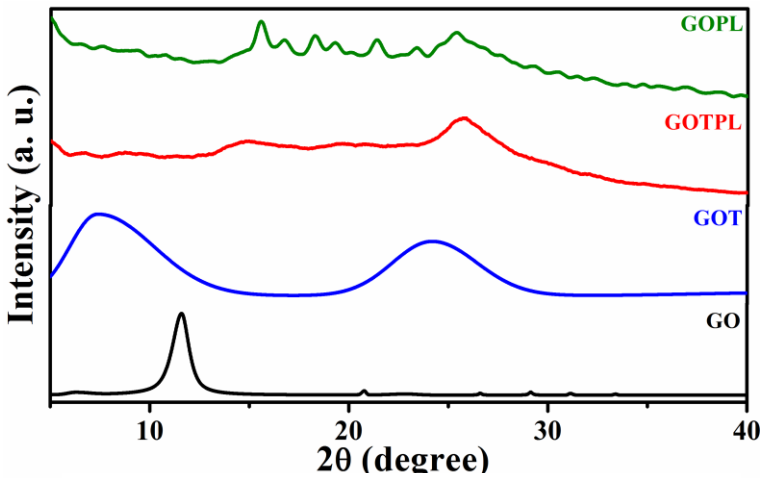

Figure 4.3: *Wide angle X-ray diffraction (WAXS) analysis of GO, GOT, GOTP, GOPL*

4.3.4. CD Spectral Analysis :

Figure 4.4 shows CD spectra for GOTP, GOPL AND GOTPL. Clearly, in case of GOTP there is no signal indicating achiral PANI chains. However, in case of GOPL dextrochirality is observed with much lower extent. In sharp contrast in case of GOTPL an intense signal is observed at 418 nm. The significant rise in chirality is attributed to the much faster rate of reaction catalysed by APQD moieties [18].

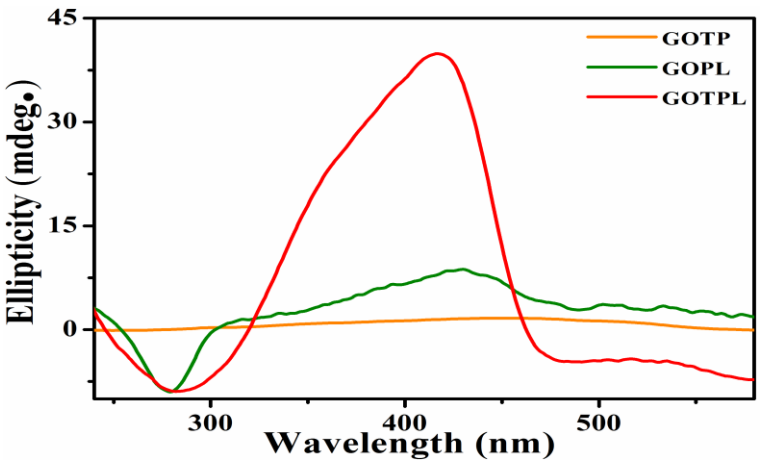

Figure 4.4: *CD Spectra analysis of GOTP, GOPL, GOTPL*

The enantioselective nature of this synthesis is shown in **Figure 4.5**, where almost a mirror image like signal is observed in cased of GOTPL and GOTPD sample when aniline polymerization is conducted either in presence of L-HCSA or D-HCSA respectively.

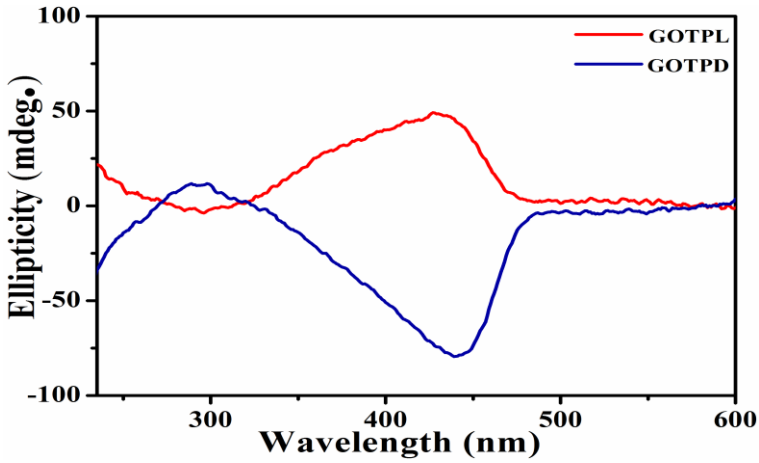

Figure 4.5: *CD Spectral analysis of GOTPL, GOTPD*

4.3.5. FESEM Analysis :

Figure 4.6 (a&b) show the FESEM images of GO and GOT with appreciably large GO sheets having micrometer size range but in case of GOT sizes have been reduced significantly. In case of GOTP **(Figure 4.6c & d)** nano structured PANI domains covering the GO surface along with relatively larger PANI cylinders or randomly connected PANI fibres are observed. On the other hand, GOPL **(Figure 4.6e)** clearly shows smooth GO surfaces without growth of any PANI chains i.e. unattached GO sheets and PANI chains. **Figure 4.6f** shows another view where randomly connected PANI fibers along with discreate appearance of non PANI attached GO sheets are apparent. However in none of the images, helicity of PANI fibres are observed. This might be due to relatively poor degree of chirality induced during reaction as observed in CD spectra. On the other hand in case of GOTPL, GO surface attached nanostructured PANI chains, along with relatively large helical PANI chains

are observed in **Figure 4.6g**. PANI fibre bundles with clearly visible helicity are observed in **Figure 4.6(g&h).**

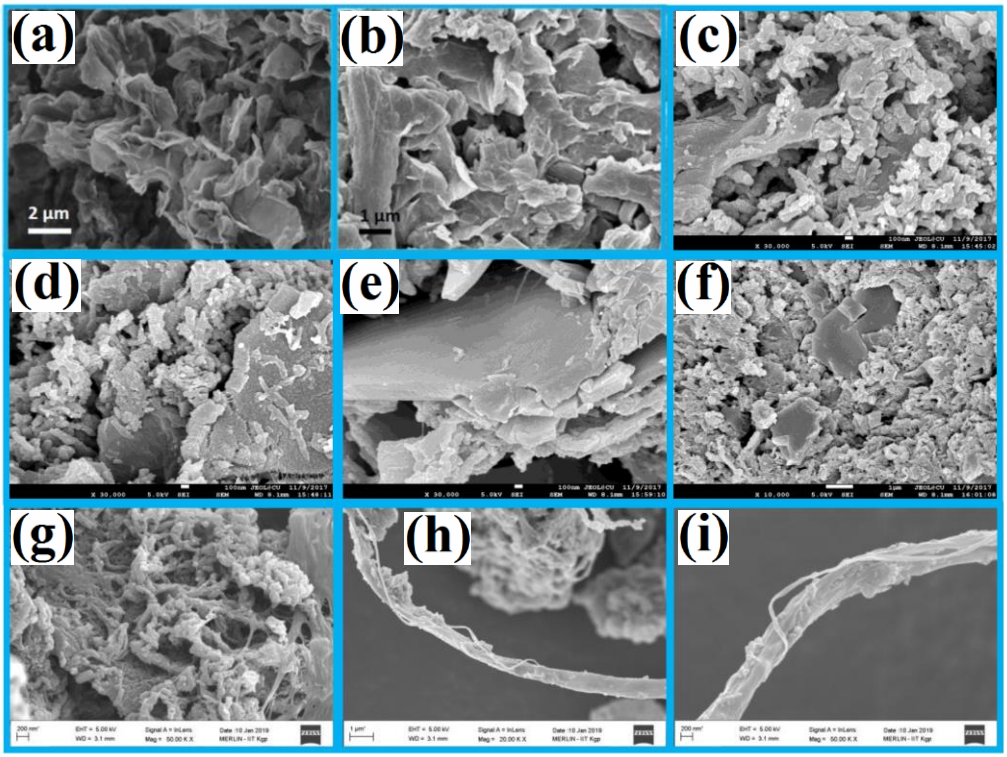

Figure 4.6: *FESEM images of (a) GO, (b) GOT, (c, d) GOTP, (e, f) GOPL and (g. h, i) GOTPL*

4.3.6. HRTEM Analysis:

In HRTEM images of GO and GOT are given in **Figure 4.7(a&b)**, where the opacity observed in large GO sheet is attributed to the π- stacked GO sheets. However, in case of GOT, due to much greater exfoliation of GO sheets transparent sheet images are observed. The representative HRTEM image of achiral GO-g-PANI nanocomposites (GOTP) given in figure 4.7c shows formation of brighter PANI domains over less bright GO sheets. In GOTPL i.e. chiral nanocomposite, helical chains are observed in **Figure 4.7d** where inset of the figure gives an enlarged view.

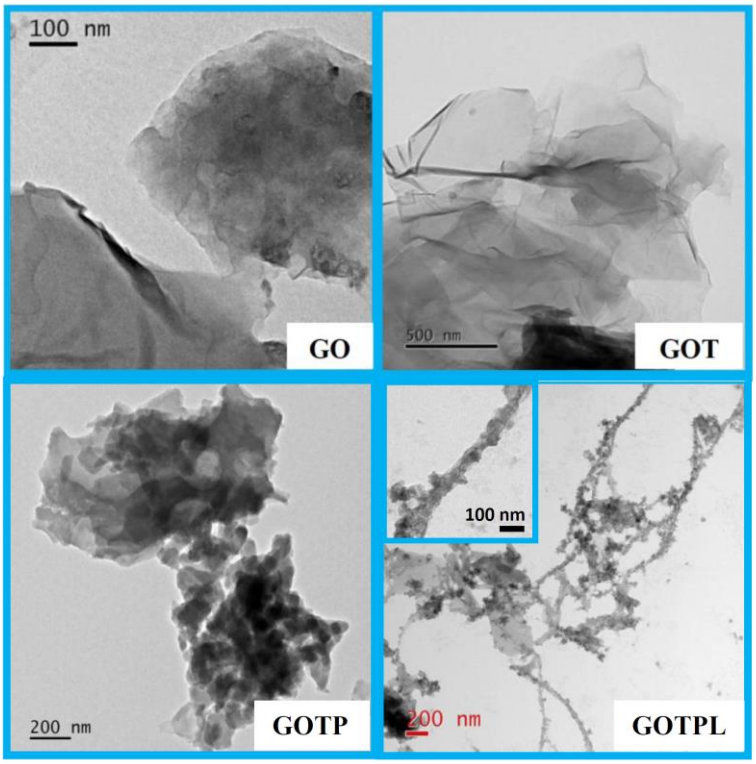

Figure 4.7: *HRTEM image of of GO, GOT, GOTP and GOTPL*

So, from the CD analysis induction of helicity is observed in case of GOTPL samples, however the degree of chirality is much less in case of GOPL. The morphological analysis also supports the conclusion.

4.3.7. Electrochemical Study:

Helical PANI fibres are expected to exert higher surface area. Therefore improved electrochemical properties are expected from the covalently attached chiral nano composites. **Figure 4.8** shows overlay of CV traces for GOPL, GOTPL and GOTP. In the CV curve appearence of quasi rectangular shape indicates operation of electrochemical double layer capacitance (EDLC). In addition, in case of GOPL, a pair of peaks near 0.19V (oxidation) and broad pair of peaks near 0.42V (oxidation) are observed. The former pair of peaks is attributed to the reversible redox tranisition between leucoemaralidine to pernigraniline state of PANI. Similar pair of peaks are also

observed in case of GOTPL and GOTP. In addition to the above redox peaks, another pair of peaks is observed at~0.72V (for GOTPL and GOTP)

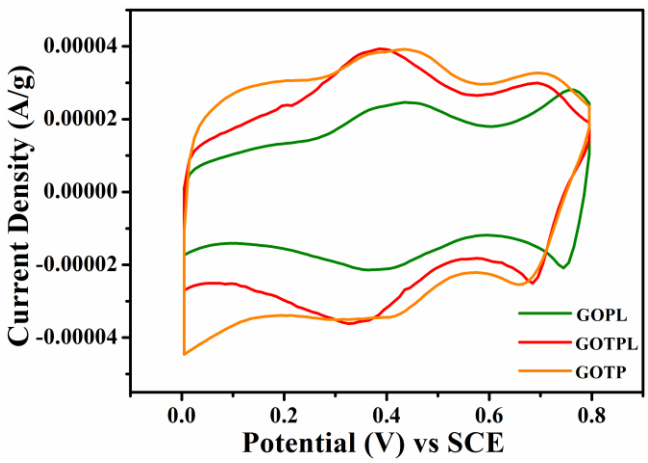

Figure 4.8: *CV curves of GOTP, GOPL and GOTPL*

and ~ 0.77V in case of GOPL. These peaks probably originate from the *ortho* coupled aniline rings present in PANI chains [31]. The significant broadness of redox peaks near 0.42V (oxidation) might be due to superposition of the redox transitions of oxygenous functionalities present on GO surface and emaralidine to pernigraniline transition of PANI chains. The area under the peak is found to increase significantly in case of GOTPL compared to GOPL. This signifies increased value of specific capacitance of GOTPL possibly due to helical PANI chains having increased surface area compared to randomly connected PANI fibres of lower degree of helicity for GOPL. However, signal area under the CV curve of GOTP is somewhat greater compared to GOTPL. This is attributed to the nanostructured PANI chain formation as observed from FESEM images. Improved specific capacitance by nano structured electrode materials is well reported in literature [32,33].

4.4. Conclusion:

Covalently grafted GO-g-PANI chiral nano composite having chiral PANI chains induced by optically pure HCSA is efficiently demonstrated. The CD and morphological analysis through FESEM and HRTEM analysis wee establish the formation of helical PANI chain formation. It has been observed that PANI chain initiation from the GO surface attached APQD moieties not only helps in covalent attachmentof the PANI chains, but also induces much higher degree of chirality. The developed synthetic protocol has found to be efficient enough to carry out the synthesis of enantioselective G0-g-PANI nano composites induced by L-HCSA or D-HCSA. The degree of chiral induction however has been found to be very much inferior in case of non covalently attached nanocomposite (GOPL) where the growth of PANI chains are not catalyzed by APQD moieties. Finally, a significant effect of covalently attached helical PANI chains from the GO surface is observed in respect of energy stotage as supercapacitor electrode. The significantly improved energy storage is attributed to the increased surface area of the chiral nano composite and synergistic effect of the covalently attached GO and PANI components. However, perhaps due to nano structuring of PANI domains in case of achral but covalently attached GO-g-PANI (GOTP) nano composite, the energy storage property has been found to be somewhat better.

4.5. References:

1. H. L. Guo, C. M. Knobler and R. B. Kaner, *Synth. Met*., 1999, **101**, 1-3.
2. E. Yashima, K. Maeda and Y. Okamoto, *Nature*, 1999, **399**, 449-451.
3. J. C. Moutet, E. Saintaman, F. Tranvan, P. Angibeaud and J. P. Utille, *Adv. Mater*., 1992, **4**, 7-8.
4. P. A. Bross, U. Schoberl and J. Daub, *Adv. Mater.*, 1991, **3**, 198-200.
5. S. A. Ashraf, L. A. P. KaneMaguire, M. R. Majidi, S. G. Pyne and G. G. Wallace, *Polymer*, 1997, **38**, 2627-2631.
6. L. A. P. Kane-Maguire, A. G. MacDiarmid, I. D. Norris, G. G. Wallace and W. G. Zheng, *Synth. Met*., 1999, **29**, 171-176.
7. H. Q. Li, A. C. Chen, S. G. Roscoe and J. Lipkowski, *J. Electroanal. Chem*., 2001, **500**, 299.
8. M. Salmon and G. Bidan, *J. Electrochem. Soc*., 1985, **132**, 1897.
9. M. Salmon, G. Bidan and E .M. Genies, *Electrochim. Acta*., 1989, **34**, 117.
10. H. Yoneyama, A. Tsujimoto and H. Goto, *Macromolecules*, 2007, **40**, 5279.
11. L. A. P. Kane-Maguire and G. G. Wallace, *Chem. Soc. Rev.*, 2010, **39**, 2545–2576.
12. M. R. Majidi, L. A. P. Kane-Maguire and G. G. Wallace, *Polymer* 1994, **35**, 3113-3115.
13. P. A. McCarthy, J. Huang, S. –C. Yang and H.-L. Wang, *Langmuir*, 2002, 18, 259-263.
14. M. Thiyagarajan, L. A. Samuelson, J. Kumar and A. L. Cholli, *J. Am. Chem. Soc*. 2003, **125**, 11502-11503.
15. S. Arnaboldi, T. Benincori, R. Cirilli, W. Kutner, M. Magni, P. R. Mussini, K. Noworytad and F. Sannicol`, *Chem. Sci.*, 2015, **6**, 1706-1711.
16. J. Huang, V. M. Egan, H. Guo, J.-Y. Yoon, A. L. Briseno, I. E. Rauda, R. L. Garrell C. M. Knobler, F. Zhou and R. B. Kaner, Adv. Mater. 2003,15, 1158-1161.
17. E. M. Sheridan and C. B. Breslin, *Electroanalysis*, 2005, **17**, 532-537.

18. W. Li and H. L. Wang, *J. Am. Chem. Soc*., **2004**, 126, 2278-2279.

19. *H. Yoneyama, A. Tsujimoto and H. Goto, Macromolecules, 2007,* ***40****, 5279.*

20. W. Li, P. A. McCarthy, D. Li, J. Huang, S.-C. Yang and H.-L. Wang, Macromolecules, 2002, **35**, 9975.

21. X. Zhang, W. Song, P. J. F. Harris, G. R. Mitchell, T. T. T. Bui and A. F. Drake, *Adv. Mater.* 2007, **19**, 1079–1083.

22. N. I. Kovtyukhova, P. J. Ollivier, B. R. Martin, T. E. Mallouk, S. A. Chizhik, E. V. Buzaneva and A. D. Gorchinskiy, *Chem. Mater*., 1999**, 11**, 771-778.

23. Y. Wei, C. Yang and T. Ding, *Tetrahedron Letters*, 1996, **37,** 731-734.

24. R. R. Mohan, S. J. Varma, M. Faisal and S. Jayalekshmi, *RSC Adv.* 2015, **5**, 5917-5923.

25. T. Remyamol, H. John and P. Gopinath, *Carbon*, 2013, **59**, 308-314.

26. L. Wang, Y. Ye, X. Lu, Z. Wen, Z. Li, H. Hou and Y. Song, *Scientific Reports*, 2013, **3**, 3568.

27. H.-L. Guo, X.-F. Wang, Q.-Y. Qian, F.-B. Wang and X.-H. Xia, *ACS Nano*, **2009**, **3,** 2653-2659.

28. F. Tuinstra and J. L. Koenig, *J. Chem. Phys*., 1970, **53**, 1126-1130.

29. A. C. Ferrari, J. C. Meyer, V. Scardaci, C. Casiraghi, M. Lazzeri, F. Mauri, S. Piscanec, D. Jiang, K. S. Novoselov, S. Roth, A. K. Geim, *PRL*, 2006**, 97,** 187401-1-187401-4.

30. L. Shi, R.-P. Liang and J.-D. Qiu, *J. Mater. Chem.*, 2012, **22**, 17196-17203.

31. Q. Liu, M. H. Nayfeh and S.-T. Yau, *J. Power Sources*, 2010**, 195**, 7480–7483.

32. G. Wang, L. Zhang and J. Zhang, *Chem. Soc. Rev*., 2012, **41**, 797–828.

33. Y.-G. Wang, H.-Q. Li and Y.-Y. Xia, *Adv. Mater*., 2006, **18**, 2619-2623